

Unveiling the spatial structure of the overionized plasma in the supernova remnant W49B

Xin Zhou^{1,2}, Marco Miceli^{3,2}, Fabrizio Bocchino², Salvatore Orlando², and Yang Chen^{1,4}

¹*Department of Astronomy, Nanjing University, Nanjing 210093, China*

²*INAF-Osservatorio Astronomico di Palermo, Piazza del Parlamento 1, 90134 Palermo, Italy*

³*Dip. di Scienze Fisiche & Astronomiche, Univ. di Palermo, Piazza del Parlamento 1, 90134 Palermo, Italy*

⁴*Key Laboratory of Modern Astronomy and Astrophysics (Nan-jing University), Ministry of Education, China*

Accepted. Received

ABSTRACT

W49B is a mixed-morphology supernova remnant with thermal X-ray emission dominated by the ejecta. In this remnant, the presence of overionized plasma has been directly established, with information about its spatial structure. However, the physical origin of the overionized plasma in W49B has not yet been understood. We investigate this intriguing issue through a 2D hydrodynamic model that takes into account, for the first time, the mixing of ejecta with the inhomogeneous circumstellar and interstellar medium, the thermal conduction, the radiative losses from optically thin plasma, and the deviations from equilibrium of ionization induced by plasma dynamics. The model was set up on the basis of the observational results. We found that the thermal conduction plays an important role in the evolution of W49B, inducing the evaporation of the circumstellar ring-like cloud (whose presence has been deduced from previous observations) that mingles with the surrounding hot medium, cooling down the shocked plasma, and pushes the ejecta backwards to the center of the remnant, forming there a jet-like structure. During the evolution, a large region of overionized plasma forms within the remnant. The overionized plasma originates from the rapid cooling of the hot plasma originally heated by the shock reflected from the dense ring-like cloud. In particular, we found two different ways for the rapid cooling of plasma to appear: i) the mixing of relatively cold and dense material evaporated from the ring with the hot shocked plasma and ii) the rapid adiabatic expansion of the ejecta. The spatial distribution of the radiative recombination continuum predicted by the numerical model is in good agreement with that observed.

Key words: hydrodynamics – ISM: individual object: W49B, G43.3–0.2 – ISM: supernova remnants – methods: numerical.

1 INTRODUCTION

W49B is one of the brightest Galactic supernova remnant (SNRs) in the radio (Moffett & Reynolds 1994) and X-ray bands (Immler & Kuntz 2005). It exhibits incomplete radio shell with centrally filled thermal X-rays (Pye et al. 1984; Smith et al. 1985), which is the characteristic of mixed-morphology supernova remnants (MM SNRs) (Rho & Petre 1998). However, at odds with typical MM SNRs, its X-ray emission is ejecta-dominated (Smith et al. 1985; Fujimoto et al. 1995; Hwang et al. 2000) and presents a central jet-like feature and a bright limb to the East (Miceli et al. 2006; Keohane et al. 2007). Near-infrared narrow-band observations revealed a barrel-shaped structure with coaxial rings (Keohane et al. 2007), probably a remnant of a bipolar wind surrounding the massive progenitor star. The X-ray jet-like

structure is along the axis of the barrel. A strip of shocked molecular hydrogen was also found in the eastern region just outside the shell, indicating that the remnant is interacting with a molecular cloud there.

Recently, a strong radiative recombination continuum (RRC) associated with H-like Fe was detected in the *SUZAKU* X-ray spectrum of W49B by Ozawa et al. (2009), thus showing the direct signature of overionization in the ejecta. Miceli et al. (2010) confirmed the RRC features by a spatially resolved spectral analysis of the *XMM-Newton* data, and found that the overionized plasma is localized in the center of the remnant and in the western region, but not in the eastern region.

The origin of such overionized recombining plasma is not well understood and rather counter-intuitive in objects

like SNRs where we mostly expect underionized plasma. Kawasaki et al. (2002) proposed that the hot interior of a SNR can, under some circumstances, cool rapidly via thermal conduction with the cooler exterior, but Yamaguchi et al. (2009) pointed out some difficulties for this scenario. By analysing the observations of IC 443, Yamaguchi et al. (2009) reexamined the time scale of thermal conduction that account for overionization in Kawasaki et al. (2002), and found that it is far longer than the remnant age. The thermal conduction alone therefore cannot account for the observed overionized plasma in IC 443, whose origin therefore remain still not well understood.

However, the estimate of Yamaguchi et al. (2009) is based on the temperature difference between hot and cold X-ray emitting component. It may still be possible (and indeed very probable) that surrounding ISM/CSM inhomogeneities (in the form of rings, large molecular clouds, cavity walls, etc.), once shocked, will give rise to a conductive thermal flux between the shocked molecular material and the inner part of the SNR. This may be indeed the case of W49B, where the higher inner temperatures than IC 443 (due to the lower age of the remnant) may further increase the effects of thermal conduction with shocked inhomogeneities.

To explain the morphology and chemical structure of W49B, two different scenarios have been proposed: either a bipolar explosion of the former supernova or a spherical supernova explosion expanding through a strongly inhomogeneous surrounding medium (Miceli et al. 2006, 2008, Keohane et al. 2007, Lopez et al. 2009). Most of these authors leave both scenarios open, but Lopez et al. (2009) strongly supports the bipolar explosion scenario, on the base of the Fe abundances measured with CIE spectral analysis in several regions of W49B. However, as shown by Ozawa et al. (2009), the abundances are different if using either CIE or overionization model. As a result, the conclusions of Lopez et al. (2009) may depend on the CIE model they used. In the light of these considerations, we believe that there is no observational evidence, at the present time, to prefer one of the two scenarios discussed above; the case of a spherical explosion expanding through an inhomogeneous medium is still realistic if considering that the plasma may be in non-equilibrium of ionization. In this paper, we focus on the reproduction of the morphology and overionization pattern of W49B by adopting the simplest SNR model, describing a spherical explosion. We will explore the alternative scenario, namely the bipolar explosion, in a forthcoming paper.

In this paper, we introduce a hydrodynamic model whose initial conditions were set up to describe appropriately W49B and investigate the physical origin of the peculiar morphology of the remnant and of the regions of overionization recently detected. The numerical model and the results are described in Sect. 2 and Sect. 3, respectively; the conclusions are summarized in Sect. 4.

2 HYDRODYNAMIC MODELING

Our model describes the evolution of an originally spherical SNR expanding through an inhomogeneous medium and, in particular, interacting with the surrounding dense clouds. The remnant evolution is modeled by numerically solving the time-dependent equations of mass, momentum, and en-

ergy conservation (as described in Orlando et al. 2005), taking into account the effects of thermal conduction (including the effects of heat flux saturation) and radiative losses from an optically thin plasma in collisional ionization equilibrium (CIE). In addition, the model includes the deviations from equilibrium of ionization induced by the dynamics as described in Reale & Orlando (2008). Although our description is not entirely self-consistent (since radiative losses are obtained assuming CIE), this does not significantly affect our results, because energy losses are dominated by transport by thermal conduction at all critical evolutionary phases (e.g. the interaction of the shock with the dense clouds, see Sect. 3) and the radiative time-scales are much larger than the age of the remnant.

We performed the calculations in a 2-D cylindrical coordinate system (r, z) using the FLASH code v2.5 (Fryxell et al. 2000), and including additional computational modules to handle the thermal conduction, the radiative losses, and the non-equilibrium of ionization (NEI) effects (see Orlando et al. 2005 and Reale & Orlando 2008 for the details of their implementation). We assumed that the fluid is fully ionized, and can be regarded as a perfect gas (with a ratio of specific heats $\gamma = 5/3$). We traced the ejecta material by considering a passive tracer initially set to 1 for pure ejecta, and 0 elsewhere.

The right panel of Fig. 1 shows the initial configuration of our model in the (r, z) plane. The setup was dictated by the results of the analysis of the X-ray and infrared observations of W49B (shown, for comparison, in the left panel of Fig. 1). We started our simulation considering a spherical remnant with radius¹ 0.5 pc. In agreement with Miceli et al. (2008), the total mass of ejecta was set to $6 M_{\odot}$ and the explosion energy to 10^{51} erg (partitioned so that $\sim 99.99\%$ of the SN energy is kinetic energy). It is worth noting that the mass of ejecta derived from the observations is subject to some uncertainties, given, for instance, the uncertainty in converting emission measure to mass. In our model, a different mass of the ejecta implies a different velocity of the ejecta (if keeping the explosion energy constant), thus influencing the energy of the shocks reflected by the clouds. This point may be important because, as shown below, the reflected shocks determine both the morphology and overionization pattern of the remnant. However, the ejecta velocity is $v_{ej} \propto m_{ej}^{-1/2}$ (where m_{ej} is the ejecta mass), so that we do not expect dramatic changes in our results if considering the uncertainty on the ejecta mass to be within a factor of 2. The ambient medium in which the remnant expands is assumed to be inhomogeneous. In particular, we focused on the coaxial rings observed by Keohane et al. (2007) in $1.64 \mu\text{m}$ [Fe II], suggesting that W49B is confined by ring-like enhanced density structures. These structures may originate from the bipolar wind of the massive progenitor star as indicated by Keohane et al. (2007), still, there are another two possibilities: the protostellar disk that had been evaporated by the ionizing radiation of the progenitor (McCray & Lin 1994), or

¹ The initial radius of the remnant has been chosen in order to have an optimal trade-off between computational time, code stability, and accuracy. In particular, we have verified that the expansion relaxes to the self-consistent free-expansion phase before the remnant hits the cloud ring, thus ensuring that our choice of 0.5 pc is optimal.

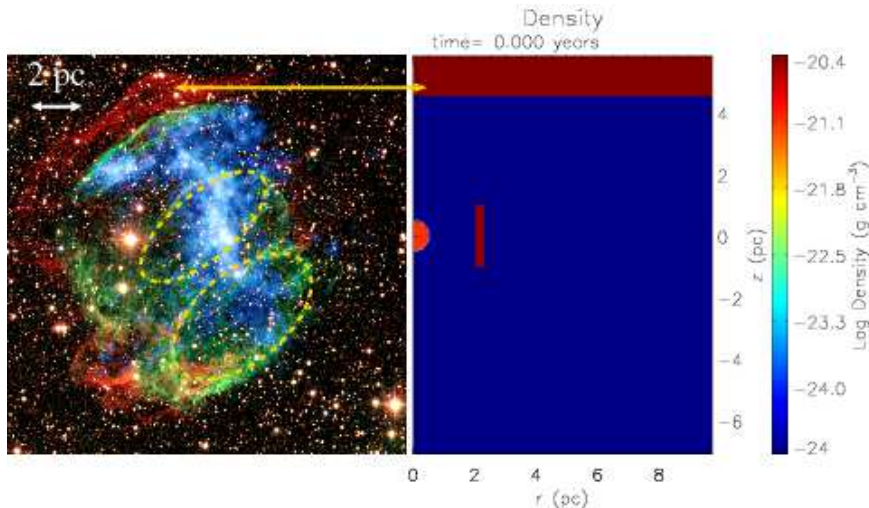


Figure 1. (*left*): Color composite image of W49B: $2.12\ \mu\text{m}$ H_2 (red), $1.64\ \mu\text{m}$ $[\text{Fe II}]$ (green), and *Chandra* X-ray (blue) (see also Miceli et al. 2006 and Keohane et al. 2007). The image has been rotated so that East is up and North is to the right. (*right*): Initial conditions of the simulation. The section in the (r, z) plane of the density distribution is shown. The model consists of a spherical SNR, a dense ring (corresponding to the coaxial rings shown in green in the left panel, and indicated by yellow ellipses), and an upper dense cloud (corresponding to the eastern molecular cloud shown in red in the left panel; the correspondence is indicated by the yellow arrows). The symmetry axis in cylindrical coordinates is at $r = 0$.

the accumulated material in the orbiting plane in a binary system. These coaxial rings are also visible in the radio continuum band (Lacey et al. 2001) and may also be the origin of the X-ray emission in the remnant (Miceli et al. 2006; Keohane et al. 2007). According to this barrel-shaped structure, a dense ring surrounding the remnant (2 pc away from the central axis) was set up in our model (its section in the (r, z) plane is shown in the right panel of Fig. 1 as a vertical bar). We fixed its density to $1600\ \text{cm}^{-3}$ in agreement with the results of Keohane et al. (2007). In addition, we accounted for the molecular H_2 cloud observed in the eastern region of the remnant, by modeling a dense wall (density $n = 2000\ \text{cm}^{-3}$, Keohane et al. 2007; see horizontal bar in the right panel of Fig. 1). It is worth emphasizing that the density values used in our model are those constrained by observations and may be affected by some uncertainties. Nevertheless we do not expect any change in our results as long as these density values remain few orders of magnitude higher than the intercloud medium. In such a case, the clouds act as walls, leading to strong reflected shocks. The tenuous intercloud medium was assumed to be isothermal ($T_{\text{ism}} = 10^4\ \text{K}$) and homogeneous (density $n_{\text{ism}} = 0.1\ \text{cm}^{-3}$). Both the dense ring and the molecular cloud are assumed to be in pressure equilibrium with the intercloud medium. Note that our model is aimed at reproducing the centrally-peaked morphology of the remnant and its pattern of overionization.

The computational domain is $\sim 10 \times 13\ \text{pc}$. At the coarsest resolution, the adaptive mesh algorithm (PARAMESH; MacNeice et al. 2000) included in the FLASH code uniformly covers the 2D computational domain with a mesh of 3×4 blocks, each with 8^2 cells. At the beginning of the simulation we allowed for 7 additional nested levels of refinement with resolution increasing twice at each refinement level. During the remnant evolution, the number of nested levels progressively decreased down to 5 at the end of the simulation. This grid configuration yields an effective resolution at the finest

level of $\sim 0.003\ \text{pc}$ at the beginning and $0.012\ \text{pc}$ at the end of the simulation. Reflecting boundary conditions were used at $r = 0\ \text{pc}$, consistently with the adopted symmetry; free outflow conditions were used elsewhere.

3 RESULTS

3.1 Hydrodynamical evolution

Fig. 2 shows the spatial distributions of density and temperature in the (r, z) plane at three different evolutionary stages; the white contours enclose the ejecta material (i.e. the fluid cells whose content is ejecta by more than 90%). During the first phase of evolution, the remnant expands through the homogeneous intercloud medium impacting on the ring-like cloud at $t \sim 250\ \text{yr}$ and on the molecular cloud at $t \sim 790\ \text{yr}$ (not shown in Fig. 2). After the interaction of the forward shock with the dense ring and the eastern dense cloud, reflected shocks develop and move backwards to the center of the remnant. At the same time, the cold cloud material evaporates under the effect of the thermal conduction, mixing with the surrounding hot shocked plasma. In the time lapse between $t \sim 1400\ \text{yr}$ and $t \sim 1700\ \text{yr}$ (upper and middle panel of Fig. 2), the hot plasma around the circumstellar ring rapidly cools down because of the mixing of the hot shocked plasma with the dense and cooler plasma evaporated from the ring. After $t \sim 1700\ \text{yr}$ (middle and lower panel of Fig. 2), the ejecta heated by the reflected shock also rapidly cool down due to their rapid adiabatic expansion². The lower panel in Fig. 2 also shows that at $t \sim 2300\ \text{yr}$ the expansion of the ejecta in the east direction

² In the central region of the remnant this adiabatic cooling is masked by the re-heating of ejecta by reflected shocks “focusing” to the center.

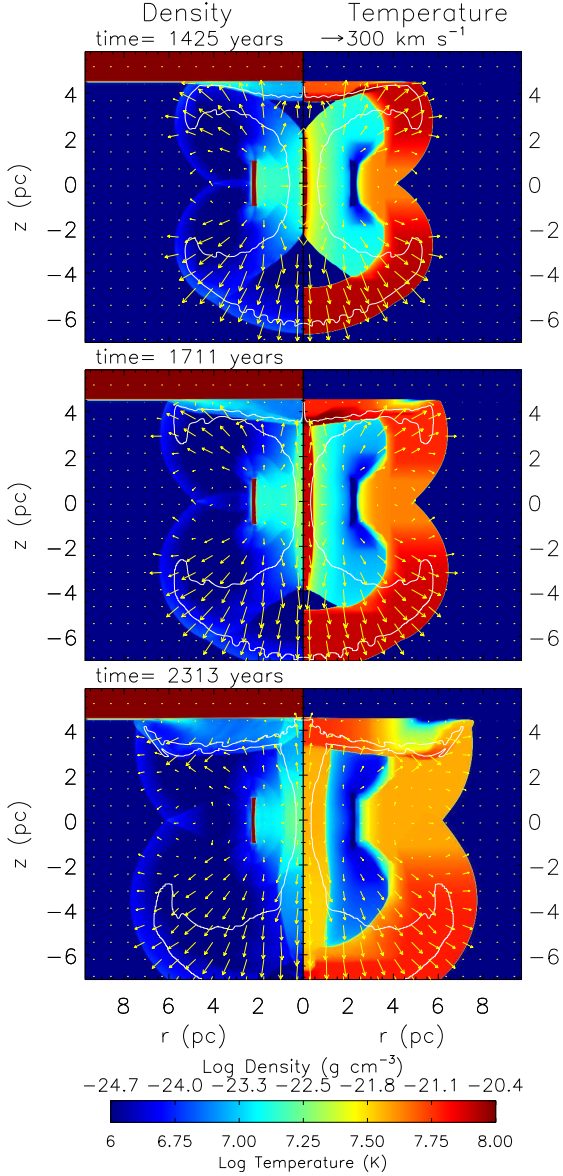


Figure 2. 2-D sections in the (r, z) plane of the mass density distribution (left) and temperature (right), both in log scale, at three different evolutionary stages (see upper left corner of each panel). The velocity arrows scale linearly with respect to the reference velocity shown in the upper right corner of the upper panel and corresponding to 300 km s^{-1} .

is hampered by the presence of the dense molecular cloud. On the contrary, the ejecta expand freely westwards, progressively cooling down.

Using Eqs. (10) and (11) in Orlando et al. (2005), we estimated the time-scales for thermal conduction and radiative losses to be a few 10^3 yr and a few 10^6 yr , respectively, in most of the intercloud region of the remnant at $t = 1400 \text{ yr}$. At later evolutionary stages, the results are the same. We conclude, therefore, that the energy losses are dominated by transport by thermal conduction at all critical evolutionary phases, and the radiative scales are much larger than the age of the remnant. The low conduction timescale are due to the large temperature contrast between shocked CSM/MC

material and the inner part of the remnant, which was not considered in the IC 443 by Yamaguchi et al. (2009).

The reflected shock from the dense ring concentrates to the center of the remnant, squeezing the ejecta there, and forming a jet-like feature with dense and hot material. We verified (with the help of an additional simulation with the same setup of that presented here but neglecting the effects of thermal conduction) that, if the thermal conduction is not included in the simulation, the ejecta are distributed over a widespread region and are not pushed backwards to the center of the remnant; as a consequence if it were not for the thermal conduction, the central jet-like feature would be too tenuous to be distinguished. At $t \sim 2300 \text{ yr}$, the central jet-like feature reaches the eastern dense cloud, and a dense and hot eastern shell (rich of ejecta) forms. The central “jet” region and the eastern “shell” region are hot enough to emit X-rays, and their surface brightness is expected to be high because of their high density and enhanced abundances. At this stage of evolution, therefore, our hydrodynamic model naturally reproduces the central jet-like feature and the eastern bright shell observed in X-rays with *XMM-Newton* and *Chandra* (Miceli et al. 2006; Keohane et al. 2007; Lopez et al. 2009). The thermal conduction and the surrounding clouds are key ingredients to reproduce the observed morphology. Since at $t \sim 2300 \text{ yr}$ both the morphology and the level of overionization (see Section 3.3) are in good agreement with X-ray observations, we suggest that this evolutionary stage can provide a good estimate for the age of W49B.

3.2 Deviations from equilibrium ionization

In this section, we address the physical origin of the overionized H-like Fe detected in W49B by Ozawa et al. (2009) and localized in the center of the remnant and in the western region, but not in the eastern region (Miceli et al. 2010). We examine the distribution of underionized/overionized plasma, by defining the iron Differential Ionization (DI) as

$$\text{DI} = \langle l \rangle_{\text{simulation}} - \langle l \rangle_{\text{equilibration}}, \quad (1)$$

$$\text{where } \langle l \rangle = \frac{\sum(f_i \times l_i)}{\sum(f_i)}$$

is the average ionization level weighted by the population fraction, f_i is the population fraction of the i th ion of Fe, l_i is the ionization level of the i th ion, and the sum is performed over all the Fe ionization stages. The subscripts “simulation” and “equilibration” in Eq. 1 refer to the value obtained in a given cell of the simulation domain and to that expected in CIE, respectively. Fig. 3 shows the population fractions of Fe versus the ionization levels derived in four different computational cells of our domain (in red, see Fig. 4 for the location of the cells), compared to those expected in CIE, at the same location (in blue). The DI parameter is a reliable indicator to distinguish the case of underionization/overionization: positive values indicate overionization (as in point #3 in Fig. 3), negative values indicate underionization (as in point #2 in Fig. 3).

The left panels of Fig. 4 show the spatial distribution of the Fe DI at the three evolutionary stages of Fig. 2, with black contours marking the ejecta overlaid. The right panels show the corresponding distributions of emission measure of

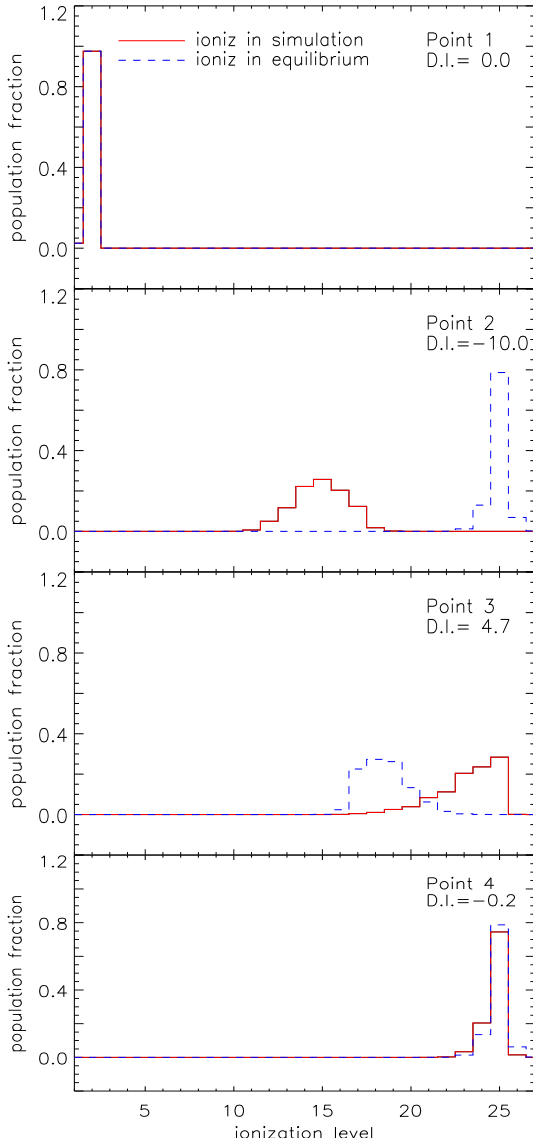


Figure 3. Ionization population plots of iron extracted from the four points indicated in the bottom panel of Fig. 4.

the [Fe xxvi] RRC (the white contours mark the value $DI = 0$). At $t \sim 1400$ yr, the overionized material (positive DI values, marked in red) is around the dense ring, and originates from the plasma previously heated by the reflected shock and rapidly cooling down because of the mixing with the cooler material evaporating from the dense ring (see Section 3.1 for a detailed description of the evolution of the system). At $t \sim 1700$ yr (middle panel of Fig. 4), conditions of overionization arise far from the ring. In this case the overionization is associated with the adiabatic cooling of the rapidly expanding ejecta (both in the east and in the west directions). At $t \sim 2300$ yr the adiabatic expansion of the ejecta in the east direction is hampered by the dense molecular cloud; the plasma there does not cool down anymore but is re-heated due to the interaction with the shock reflected by the molecular cloud. As a consequence, the conditions of overionization there are not present anymore. On the contrary, they are still present in the western region where the plasma keeps to expand freely. Since the time $t \sim 1700$ yr

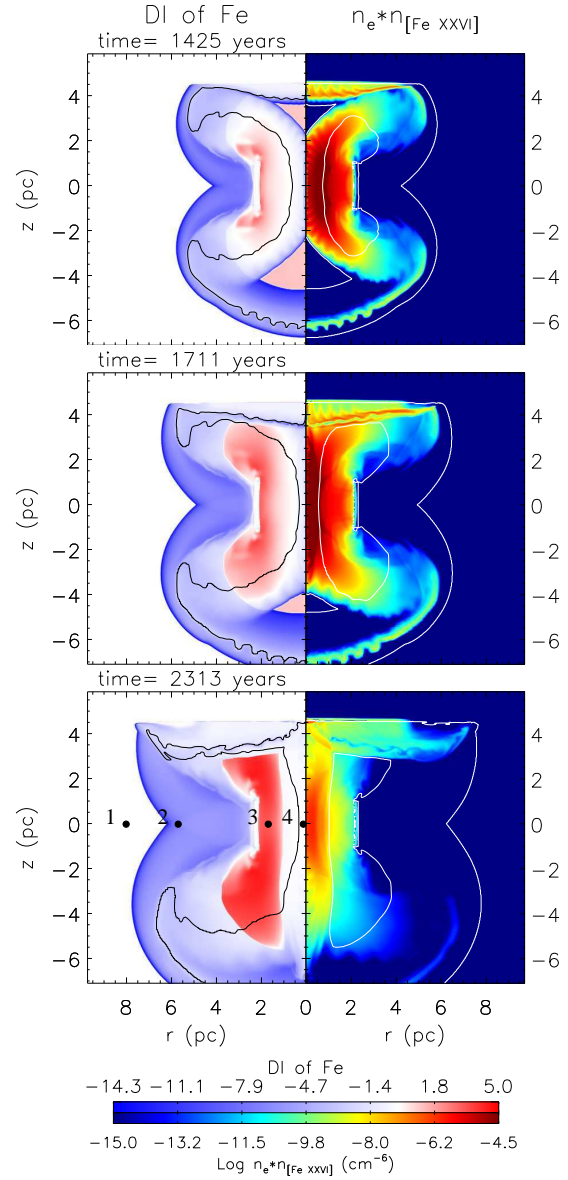


Figure 4. 2-D sections in the (r, z) plane of the differential ionization of iron (left; see the text for the definition of DI) and the emission measure of [Fe xxvi] RRC (right), at the three evolutionary stages as in Fig. 2 (see upper left corner in each panel). The black contours (on the left) enclose the ejecta material, the white contours (on the right) mark the value $DI = 0$. Positive values of DI (marked in red in the left panels) indicate the case of overionization; negative values (blue) indicate the case of underionization. In the calculation of the emission measure of [Fe xxvi] line emission, we have assumed that the metal abundance of iron is $5 Z_{\odot}$, according to Miceli et al. (2006). The circular points in the third panel are the points selected for showing the ionization population in Fig. 3.

and onwards, the overionized plasma is composed by both shocked ISM and ejecta, as it is shown by the intersection of the red region and the ejecta contours in the left middle and left bottom panels of Fig. 4.

3.3 Strength of radiative recombination continuum (RRC)

We compare our model results with X-ray observations of W49B by computing, for each computational cell, the ratio ρ between the X-ray luminosity of the [Fe xxvi] RRC and the thermal bremsstrahlung emission. The diagnostic power of this ratio consists in getting the information about the strength of the RRC. In fact, high values of ρ qualitatively corresponds to regions where the RRC edge has the highest probability of being observed. According to the radiative recombination model in ATOMDB (see Smith & Brickhouse 2002) v1.3.1, the luminosity of the [Fe xxvi] RRC is

$$L_{\text{RRC}} \propto n_e n_{[\text{Fe xxvi}]} \exp\left(-\frac{E_\gamma - E_{\text{edge}}}{kT}\right) T^{-3/2} \quad (2)$$

where E_{edge} is the K-edge energy of the [Fe xxv] which is 8.83 keV and E_γ is the energy of the emitted photon which is set to be equal to E_{edge} in our strength examination. The approximation of the luminosity of thermal bremsstrahlung emission is proportional to (Longair 1994):

$$\begin{cases} T^{-1/2} n_e n_i \log\left(\frac{kT}{E_\gamma}\right) \exp\left(-\frac{E_\gamma}{kT}\right), & \text{when } E_\gamma < kT \\ T^{-1/2} n_e n_i \left(\frac{E_\gamma}{kT}\right)^{1/2} \exp\left(-\frac{E_\gamma}{kT}\right), & \text{when } E_\gamma \gg kT. \end{cases} \quad (3)$$

The ratio ρ between the luminosity of the [Fe xxvi] RRC and the thermal bremsstrahlung emission is proportional to:

$$\begin{cases} \frac{n_{[\text{Fe xxvi}]}}{n_i} T^{-1} \log\left(\frac{kT}{E_\gamma}\right)^{-1} \exp\left(\frac{E_{\text{edge}}}{kT}\right), & \text{when } E_\gamma < kT \\ \frac{n_{[\text{Fe xxvi}]}}{n_i} T^{-1} \left(\frac{kT}{E_\gamma}\right)^{1/2} \exp\left(\frac{E_{\text{edge}}}{kT}\right), & \text{when } E_\gamma \gg kT. \end{cases} \quad (4)$$

To compute ρ we also assume a pure ejecta plasma which can be mimicked by setting the abundances to high values, we explored the Fe abundance in the range of 1–10000 Z_\odot , while we assumed solar abundance for ISM and CSM. We adopted the ejecta tracer as a factor to evaluate the real Fe abundance in the computational cells where ejecta and ISM are mixed together. We found that different choices of the abundance of pure ejecta have only secondary effects on ρ . In particular, the [Fe xxvi] RRC is already clearly visible at 5 Z_\odot (the value found by Miceli et al. (2006) for W49B), as it is shown by the map of ρ in the (r, z) plane at $t \sim 2300$ yr presented in Fig. 5, and it is more visible with larger abundance. The [Fe xxvi] RRC is mainly visible at the center and in the western region (corresponding to the western part of W49B), in good agreement with the observations (Miceli et al. 2010).

4 SUMMARY AND CONCLUSIONS

We modeled the evolution of W49B taking into account, for the first time, the mixing of ejecta with the inhomogeneous circumstellar and interstellar medium, the thermal conduction, the radiative losses from optically thin plasma, and the deviations from equilibrium of ionization induced by the dynamics. Our model is suited to address the still pending issue of the origin of overionized plasma in W49B whose direct detection has been recently reported. The initial conditions of the model were set up according to the

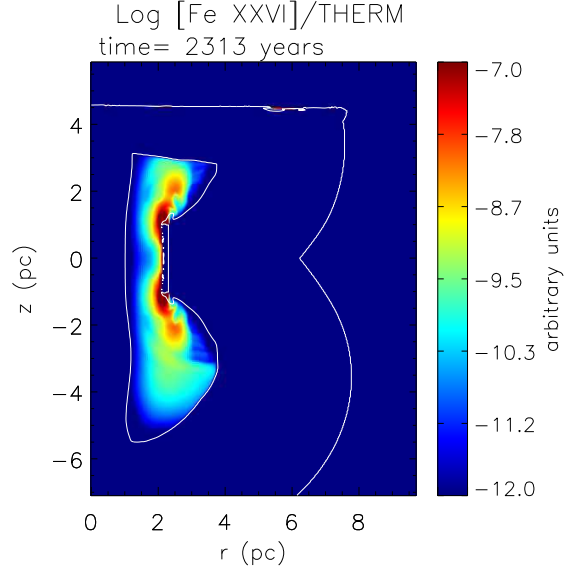


Figure 5. Map of the ratio between the luminosities of RRC of [Fe xxvi] and thermal bremsstrahlung emission in the (r, z) plane, with the contour marking the value $DI = 0$ the same as the contour in the right half of each panel in Fig. 4. The luminosities of RRC of [Fe xxvi] and thermal bremsstrahlung emission are in arbitrary units. The ejecta material is considered to be with the abundance of 5 Z_\odot , corresponding to that found by Miceli et al. (2006). The larger the ratio the more visible the RRC.

observational constraints derived for W49B and for its inhomogeneous circumstellar environment.

Our model recovered the X-ray morphology of the remnant (the jet-like feature and a sharp shell behind the molecular cloud highlighted by XMM and Chandra observations; Miceli et al. 2006; Keohane et al. 2007) and the spatial distribution of the overionized ejecta (localized in the center of W49B and in its western region; Miceli et al. 2010). We found that the thermal conduction plays an important role in the evolution of the system, since it induces the evaporation of a non-negligible fraction of the cold and dense cloud material that mixes with the hot surrounding shocked medium, and promotes the formation of the characteristic central bright feature of this mixed morphology remnant (see Fig. 2). Further more, as in W49B, similar coaxial rings and jet-like features are also present in the X-ray emission in SNR 3C397 (rings in Jiang 2009; jets in Safi-Harb et al. 2005 and Jiang & Chen 2010) that is interacting with a complicated molecular environment (Jiang et al. 2010); our simulation may also provide a similar (but qualitative) explanation for the structures in 3C397.

Our model predicts that overionization originates in the remnant due to the rapid cooling of the hot plasma originally heated by the shock reflected from the dense ring toward the center of the remnant. We found two different classes of overionized plasma: one consists of shocked interstellar medium (ISM), the other of a mixture of shocked ISM and ejecta material. These two classes are associated with different cooling processes, respectively: i) the mixing of hot shocked plasma with the cooler dense material evaporated from the ring, and ii) the rapid adiabatic expansion of plasma. In particular, the overionization of the ejecta (observed in X-rays)

is due to their rapid free expansion that follows their early heating.

In this paper we adopted the simplest configuration of the initial SN explosion, by considering a spherical symmetry. Nevertheless, this simple configuration together with the inhomogeneities of the interstellar medium reproduce the morphology and overionization pattern of the remnant quite naturally. Our model suggests that the bipolar morphology of W49B (e.g. its jet-like feature) could be an hydrodynamic effect originating from the interaction of shocks reflected by the surrounding clouds. The model indicates that the plasma in the remnant is in NEI, and it could explain the unexpected Fe abundances found by Lopez et al. (2009) in terms of overionization of the ejecta. It is worth emphasizing that our analysis does not rule out the possibility of a bipolar explosion in origin. This alternative scenario deserve a further investigation in a forthcoming paper.

On the basis of the morphology and conditions of overionization, we derived $t \sim 2300$ yr as a good estimate for the age of W49B. Our model shows that at this evolutionary stage, there is more overionized plasma in the region where the ejecta expansion is not hampered. The strength of the RRC of [Fe xxvi] and its spatial distribution are consistent with the X-ray observations. Our findings support, therefore, the new idea that surrounding molecular clouds could be necessary ingredients to reproduce the peculiar morphology, ionization conditions, and abundance patterns of MM SNRs. High resolutions maps of RRC emission are needed to confirm this scenario or other possible interpretations like in Yamaguchi et al. (2009).

ACKNOWLEDGMENTS

We thank the anonymous referee for the valuable comments on our previous draft. XZ would like to thank the friendly atmosphere at Osservatorio Astronomico di Palermo. The software used in this work was in part developed by the DOE-supported ASC / Alliance Center for Astrophysical Thermonuclear Flashes at the University of Chicago, using modules for non-equilibrium ionization, thermal conduction, and optically thin radiation built at the Osservatorio Astronomico di Palermo. The simulation was performed on the SCAN (Sistema di Calcolo per l'Astrofisica Numerica) HPC facility of the INAF-Osservatorio Astronomico di Palermo. This work was partially supported by NSFC grants 10725312 and 10673003 and the China 973 Program grant 2009CB824800. This work was partially supported by the ASI-INAF contract n. I/009/10/0.

REFERENCES

Fryxell, B., Olson, K., Ricker, P., et al. 2000, *ApJS*, 131, 273
 Fujimoto, R., Tanaka, Y., Inoue, H., et al. 1995, *PASJ*, 47, L31
 Hwang, U., Petre, R., & Hughes, J. P. 2000, *ApJ*, 532, 970
 Immler, S., & Kuntz, K. D. 2005, *ApJ*, 632, L99
 Jiang, B. 2009, Ph.D. dissertation, Nanjing University
 Jiang, B., & Chen, Y. 2010, *Science in China G: Physics and Astronomy*, 53, 267
 Jiang, B., Chen, Y., Wang, J., Su, Y., Zhou, X., Safi-Harb, S., & DeLaney, T. 2010, *ApJ*, 712, 1147

Kawasaki, M. T., Ozaki, M., Nagase, F., Masai, K., Ishida, M., & Petre, R. 2002, *ApJ*, 572, 897
 Keohane, J. W., Reach, W. T., Rho, J., & Jarrett, T. H. 2007, *ApJ*, 654, 938
 Lacey, C. K., Lazio, T. J. W., Kassim, N. E., et al. 2001, *ApJ*, 559, 954
 Longair, M. S. 1994, Cambridge University Press, Cambridge (UK)
 Lopez, L. A., Ramirez-Ruiz, E., Pooley, D. A., & Jelltema, T. E. 2009, *ApJ*, 691, 875
 MacNeice, P., Olson, K. M., Mobarry, C., de Fainchtein, R., & Packer, C. 2000, *Comp. Phys. Comm.*, 126, 330
 McCray, R., & Lin, D. N. C. 1994, *Nature*, 369, 378
 Miceli, M., Decourchelle, A., Ballet, J., Bocchino, F., Hughes, J. P., Hwang, U., & Petre, R. 2006, *A&A*, 453, 567
 Miceli, M., Decourchelle, A., Ballet, J., Bocchino, F., Hughes, J., Hwang, U., & Petre, R. 2008, *Adv. Space Res.*, 41, 390
 Miceli, M., Bocchino, F., Decourchelle, A., Ballet, J., & Reale, F. 2010, *A&A*, 514, L2
 Moffett, D. A., & Reynolds, S. P. 1994, *ApJ*, 437, 705
 Orlando, S., Peres, G., Reale, F., Bocchino, F., Rosner, R., Plewa, T., & Siegel, A. 2005, *A&A*, 444, 505
 Ozawa, M., Koyama, K., Yamaguchi, H., Masai, K., & Tamagawa, T. 2009, *ApJ*, 706, L71
 Pye, J. P., Thomas, N., Becker, R. H., & Seward, F. D. 1984, *MNRAS*, 207, 649
 Reale, F. & Orlando, S. 2008, *ApJ*, 684, 715
 Rho, J., & Petre, R. 1998, *ApJ*, 503, L167
 Safi-Harb, S., Dubner, G., Petre, R., Holt, S. S., & Durouchoux, P. 2005, *ApJ*, 618, 321
 Smith, A., Peacock, A., Jones, L. R., & Pye, J. P. 1985, *ApJ*, 296, 469
 Smith, R. K., & Brickhouse, N. S. 2002, *Physics Underlying the ATOMDB* (Cambridge, MA: Chandra X-Ray Center), <http://cxc.harvard.edu/atomdb/physics/plasma/plasma.html>
 Yamaguchi, H., Ozawa, M., Koyama, K., Masai, K., Hiraga, J. S., Ozaki, M., & Yonetoku, D. 2009, *ApJ*, 705, L6